Photocatalytic ozonation under visible light for the remediation of water effluents and its integration with an electro-membrane bioreactor

*Diego Toledano Garcia,[1] Lütfiye Y. Ozer,[1] Francesco Parrino,[2] Menatalla Ahmed,[1] Grzegorz Przemyslaw Brudecki,[3] Shadi W. Hasan,[1] Giovanni Palmisano[1]**

[1] Department of Chemical Engineering, Khalifa University of Science and Technology - Masdar Institute, Masdar City, PO BOX 54224, Abu Dhabi, United Arab Emirates. Email: *gpalmisano@masdar.ac.ae

[2] Dipartimento di Energia, Ingegneria dell'Informazione e Modelli Matematici (DEIM), University of Palermo, Viale delle Scienze Ed. 6, Palermo (90128), Italy.

[3] Department of Research Laboratories, Khalifa University of Science and Technology - Masdar Institute, Masdar City, PO BOX 54224, Abu Dhabi, United Arab Emirates.

Abstract

Photocatalysis and photocatalytic ozonation under visible light have been applied for the purification of a complex aqueous matrix such as the grey water of Masdar City (UAE), by using N-doped brookite-rutile catalysts. Preliminary runs on 4-nitrophenol (4-NP) solutions allowed to test the reaction system in the presence of a model pollutant and to afford the relevant kinetic parameters of the process. Subsequently, the remediation of grey water effluent has been evaluated in terms of the reduction of total organic carbon (TOC) and bacterial counts. The concentration of the most abundant inorganic ionic species in the effluent has been also

monitored during reaction. Photocatalytic ozonation under visible light allowed to reduce the TOC content of the grey water by ca. 60% in the optimized experimental conditions and to reduce the total bacterial count by ca. 97%. The extent of TOC mineralization reached ca. 80% when the photocatalytic ozonation occurred downstream to a preliminary electro-membrane bioreactor (eMBR). Coupling the two processes enhanced the global efficiency. In fact, the eMBR treatment lowered the turbidity and the organic load of the effluent entering the photocatalytic ozonation treatment, which in turn enhanced the extent of purification and disinfection.

Keywords

Photocatalytic ozonation; visible light; grey water; electrically enhanced membrane bioreactor; Nitrogen-doped Titanium dioxide

1. Introduction

Photocatalysis has attracted considerable interest as a promising tool for environmental remediation (León et al., 2017; Ohno and Tsubota, 2010; Vilar et al., 2017). The oxidizing ability of this technology is due to the photogeneration of highly active radical species such as hydroxyl radicals, which unselectively degrade almost every organic pollutant with few exceptions (Kisch, 2014). TiO_2 is the most used and studied photocatalyst to this aim. Indeed, its chemical (photo)stability, abundancy and low cost, along with the possibility of tailoring its properties according to the desired application, justify its widespread use in the relevant literature (Augugliaro et al., 2010; Dolat et al., 2013). At least three main issues limited so far large scale applications of TiO_2 photocatalysis: (i) TiO_2 is not able to absorb the visible fraction of the solar spectrum, (ii) photocatalytic runs on real complex matrices generally show low reaction rates, (iii) the process cost is not sufficiently competitive, being the current technology still not mature for full scale applications in grey water treatment.

By taking into account that UV light only represents ca. 4% of the solar spectrum, extending the light harvesting ability of TiO_2 to the visible range is highly desirable, as it would imply an efficient exploitation of solar energy. Different techniques have been proposed for TiO_2 sensitization (Pelaez et al., 2012). Among them nitrogen doping combines versatile, easy and inexpensive preparation procedures, good visible light responsiveness and stability of the photocatalyst under irradiation. The second issue to be taken into account is related to the low reaction rates observed when photocatalysis is applied to real, complex aqueous matrices. The main factors affecting photocatalytic efficiency are high salinity and turbidity or high pollutants load. Salts dissolved in water drastically diminish the oxygen solubility with a major effect on the charge transfer mechanisms. On the other hand, turbidity reduces the penetration of light

through the suspension and the availability of photons as reactants. High organic load may as well influence the light distribution but also poison the photocatalyst by irreversibly occupying the active sites. To overcome these problems photocatalysis has been proposed coupled with other advanced oxidation techniques (Ahmadi et al., 2015; Garcia-Segura and Brillas, 2017; Tseng et al., 2012), with physical methods (Cataldo et al., 2016), or it has been applied as a tertiary water treatment after a biological process (Bernabeu et al., 2011; Borges et al., 2014). One of the most promising methods is the integration of photocatalysis with ozonation (Parrino et al., 2014). It has been demonstrated that photocatalytic ozonation affords reaction rates higher than the sum of those obtained by considering the single technologies acting separately (Parrino et al., 2015). This is mainly due to the higher electrophilicity of ozone with respect to oxygen. In fact, generation of one hydroxyl radical requires three electrons (i.e. photons) in the presence of oxygen and only one electron in the presence of ozone (Agustina et al., 2005). Plenty of articles report on photocatalytic ozonation for the degradation of model pollutants such as phenols (Ardizzone et al., 2011), formic acid (Wang et al., 2002) or methanol (Mena et al., 2012) among others. Fewer studies target the photocatalytic ozonation of real wastewater effluents, like winery wastewater (Gimeno et al., 2007), reused water (Zou and Zhu, 2008) or seawater (Camera-Roda et al., 2018). Even less are the investigations on photocatalytic ozonation under visible light for the degradation of pollutants such as pesticides (3,6-dichloro-2-methoxybenzoic acid) (Maddila et al., 2016) and other compounds like oxalic acid (Mano et al., 2015; Pan et al., 2015) at laboratory scale.

To the best of our knowledge the use of photocatalytic ozonation under visible radiation for the treatment of real effluents such the one here investigated, has not been comprehensively studied earlier. A nitrogen-doped TiO_2 (N-TiO_2) sample, comprised of brookite and rutile phase,

has been prepared according to Pikuda et al. (2017) and used for the present investigation. Our results have been compared to those obtained with the commercial TiO_2 Evonik P25, which is widely considered a benchmark.

Given that visible photocatalytic ozonation has been rarely studied, in particular by using N-doped TiO_2, we have first investigated the possibility to perform such a treatment through the degradation of a model compound, which is 4-nitrophenol (4-NP), in order to assess the reaction conditions and to determine some relevant kinetic parameters. 4-NP is a stable, water soluble, bio-recalcitrant compound, representing an issue for the environment and the public health and whose photocatalytic degradation has been deeply studied in literature. Afterwards, the same visible light photocatalytic ozonation was applied to grey water collected in Masdar City (Abu Dhabi, UAE) and, finally, it was performed downstream to an electrically enhanced membrane bioreactor (eMBR). No reports in literature approached the coupling of advanced oxidation processes with eMBR for the treatment of raw grey water effluents. The eMBR is a combination of biological process, membrane filtration and elektrokinetics (Giwa and Hasan, 2015a, 2015b, Hasan et al., 2014, 2012). This allows some electrochemical phenomena to happen such as electrocoagulation, electroosmosis and electrophoresis, enhancing the effectiveness of this treatment when compared with traditional membrane bioreactors (Ensano et al., 2016). The preliminary treatment by means of eMBR upstream to the photocatalytic ozonation process produced several advantages, thus increasing the efficiency of the global process as discussed throughout the paper.

2. Experimental

2.1. Chemicals, catalysts and water

All the chemicals were used as received without further purifications. The catalyst chosen for the present investigation was a N-TiO_2 sample (labeled as 0.8% N-TiO_2) obtained by a sol-gel method described by Pikuda et al. (2017). Briefly, Ti (IV) butoxide (Sigma Aldrich puriss. p.a.) was used as the titanium precursor in an acidic hydro-alcoholic solutions in the presence of HCl (Sigma Aldrich, 37%) and 2-propanol (Sigma Aldrich, puriss. p.a.). Ammonium nitrate (Sigma Aldrich, puriss. p.a.) was added as the nitrogen precursor in order to obtain 0.8% in weight of nitrogen doping in the final sample. This nitrogen content is reported by Pikuda to show the best photocatalytic performance. The photocatalyst obtained as a result of this preparation is a mixture of brookite (20%), rutile (18.5%), and amorphous phase (61.5%) with a specific surface area (SSA) of 57.6 m^2 g^{-1}. For the sake of comparison, pure TiO_2 Evonik P25 (ca. 80% anatase and 20% rutile phase, SSA: 50 m^2 g^{-1}) was used as a benchmark.

Prior to the photocatalytic treatment, the grey water was collected on 18th May 2016, filtered in a vacuum pump system with a Whatman filter (pore size of 1.2 μm) and characterized. The characterization of the grey water before and after filtration is summarized in Table S1.

Photocatalysis and/or ozonation runs were carried out only on filtered grey water.

Given the limited rate of photocatalytic reactions on untreated grey water, the dilution was needed to assess the degradation results in a reasonable time. On the other hand, dilution was not necessary in the integrated system, i.e. when photocatalytic ozonation was performed downstream to the eMBR treatment.

2.2. Photocatalytic reactor: setup and procedures

A scheme of the experimental setup used for the reactivity tests is shown in Figure 1. Runs were carried out in a pressurized semi-batch reactor of 0.75 L made of Pyrex glass, to ensure the transmittance of radiation through its walls. The parts of the reaction system are indicated with letters in Figure 1.

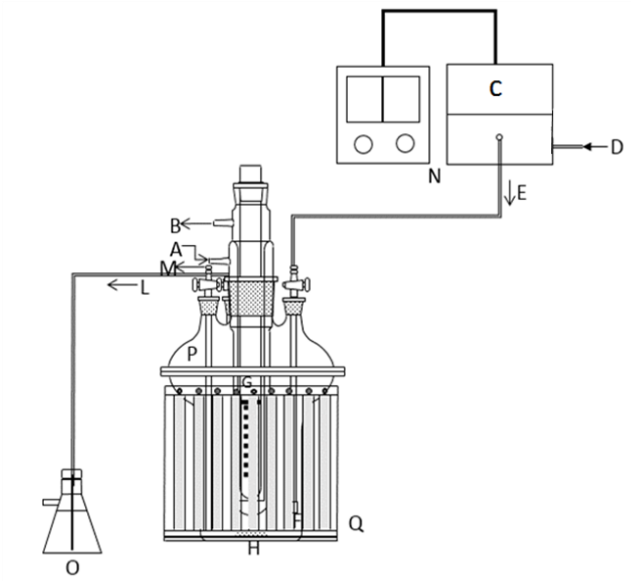

Entry	Description	Entry	Description
A	Coolant inlet	**H**	Stirring magnet
B	Coolant outlet	**L**	Outlet gas
C	Ozonator	**M**	Syringe
D	Oxygen inlet	**N**	Vol. flow controller
E	Gas mixture outlet	**O**	Erlenmeyer flask
F	Gas inlet diffuser	**P**	Pyrex glass reactor
G	Internal LED lamp	**Q**	External LED lamp

Figure 1. Scheme and parts of the semi-batch reaction system used in the experiments.

The radiation sources were UV-free visible LED strips (SMD 3014) with the emission band between 425 and 750 nm (Figure S1). The lamps were placed outside the external walls of the reactor and inside a housing in Pyrex immersed in the reacting suspension and surrounded by a thimble where recirculating cooling water ensured a constant operational temperature and prevented LED strips from overheating. The absorbed electric power of the internal and external lamps were 20.54 and 70.2 W, respectively. The radiant power of both internal and external LED systems was measured separately: the external one was 630 W m^{-2}, measured at the external wall of the reactor, while the internal was 179 W m^{-2}, measured at the external wall of the thimble containing the cooling fluid. The flow rate of oxygen bubbling through the suspension was set at

142 100 mL min^{-1} by using a mass flow controller (Bronkhorst F-201 CV) to ensure saturation of
143 oxygen in the solution.

144 Ozone was produced from pure oxygen in an ozone generator (Aeraque Microlab 1AQ). The
145 operating conditions of the generator were fixed in order to obtain an ozone concentration in the
146 gaseous stream of 56.4 g m^{-3} (measured at 1 bar), corresponding to a total production of ozone of
147 1.7 g h^{-1} at the operating flowrate of the equipment (0.4 L min^{-1}).

148 The amount of catalyst used in each run was 1.5 g L^{-1} for 0.8% N-TiO_2, at which the light
149 transmittance measured at the external wall of the reactor was ca. 40% compared to the one in
150 the absence of the catalyst; the catalyst amount was not further increased to prevent
151 sedimentation. P25 was used with an amount of 0.85 g L^{-1}, which produced a similar
152 transmittance. This amount allowed to normalize the intensity of photons being absorbed and
153 scattered by the suspension and to enable comparison of the results. The initial concentration of
154 4-NP ranged between 1 and 8 ppm and the pH was the natural one, i.e. ca. 6. The suspension was
155 sonicated for 10 min to ensure good dispersion of the catalyst and left under stirring in the
156 presence of gas bubbling in dark conditions for 1 h in order to achieve thermodynamic
157 adsorption-desorption equilibrium. To monitor dark adsorption, a sample of the initial solution
158 was withdrawn before the ignition of the lamp. Once the lamps were switched on, samples were
159 taken at fixed time intervals, filtered to separate the catalyst with PVDF syringe filters (0.2 μm)
160 and immediately analyzed.

161

162 ***2.3. eMBR setup***

163 The eMBR treatment upstream to some photocatalytic ozonation runs was performed by
164 means of a lab-scale continuous mode eMBR, designed by Giwa et al. (2015) and Hasan et al.

(2014) for the treatment of municipal grey water collected from Masdar City at an effluent flow rate of 40 L d^{-1}. The effective volume of the reacting liquid was 22.5 L. The membrane employed was a flat sheet submerged microfiltration (MF) membrane with a pore size of 0.4 μm supplied by KUBOTA Corporation. The material of the membrane consisted of acrylonitrile butadiene styrene (ABS), polypropylene (PP), polyethylene terephthalate, and chlorinated polyethylene at a proportion of 1:2:2:2. A constant current density of 10 A m^{-2} was maintained throughout the experiment by adjusting the voltage knob, and an intermittent current (5 min ON, 15 min OFF) was supplied by using an electronic timer. The chosen configuration was A-C-M-C-A (A stands for anode, C stands for cathode, and M stands for membrane). The anodes and cathodes were made of aluminum and stainless steel, respectively. The sludge inoculum was obtained from an MBR water treatment plant at Masdar City, with an initial average mixed liquor suspended solids (MLSS) of 2200 mg L^{-1}.

2.4. Analytical techniques

A UV-VIS spectroscopy (Shimadzu UV-2600) at 315 nm and a TOC instrument (Shimadzu TOC-L) were employed to retrieve the 4-NP concentration and its mineralization degree, respectively. Preliminarily, a HPLC equipped with an Acclaim-120 C18 Reversed-phase LC column, eluent: 33% water, 33% acetonitrile, 33% methanol, 1% 2M ammonium acetate, flowrate 0.2 mL min^{-1}, was used to verify that the absorbance recorded at the UV-VIS spectrophotometer at 315 nm gives a proper measurement of 4-NP concentration, without being significantly affected by organic oxidized intermediates. The reproducibility of the photocatalysis and/or ozonation runs was always over 95%, replicated at least 2 times.

The purification extent of grey water was monitored by measuring the TOC content (Shimadzu TOC-L) of samples taken at fixed intervals of times and by the total bacteria count (TBC) method. The latter analysis was carried out by the plate count agar method. The culture media, consisting of 10 g Tryptone, 5 g Yeast extract, 5 g NaCl and 15g agar in 1 L water, were autoclaved for 15 min at 121°C to ensure the sterility and poured in the sterile petri dishes. An aliquot (100 µL) of samples was cultured in LB agar plate for 48 h at 37°C. Serial dilutions was used to obtain more precise number of the bacterial colonies defined as colony forming units per mL (CFU). The ions content was also analyzed by means of a Thermo Scientific Dionex ICS-5000 ion chromatograph.

2.5. Kinetic assessment of 4-NP degradation

The kinetics of 4-NP degradation were assessed through Langmuir-Hinshelwood (L-H) model. Eq. 1 shows the general expression of the L-H kinetics:

$$r_H = -\frac{1}{S}\frac{dn_p}{dt} = k''\theta_p\theta_o \quad (1)$$

where the rate of reaction r_H is a function of the fractional surface coverage of pollutant θ_p and the fractional surface coverage of the gas (oxygen or ozone) θ_o, multiplied by a second order kinetic constant k''. In the experimental conditions under which 4-NP was oxidized, saturation of gas in the aqueous media may be safely hypothesized, so that the fractional surface coverage of gas θ_o can be considered constant. Accordingly, a new pseudo first order constant k, product of k'' and θ_o, can be defined as shown in Eq. 2, where the dependence on the reactor volume V, the specific surface area of the catalyst S_c, and the mass of catalyst M have been introduced.

$$r_H = -\frac{1}{S}\frac{dn_p}{dt} = -\frac{V}{S_C M}\frac{dC_P}{dt} = k\,\theta_p \quad (2)$$

The fractional surface coverage of the pollutant (Eq. 3) is a function of its concentration in the liquid phase C_p, experimentally obtained, of K_a, i.e. the adsorption constant of the pollutant on the catalyst, and of C_i and K_i, which are analogously defined for the intermediate species generated during the reaction.

$$\theta_p = \frac{K_a C_p}{1+K_a C_p+\Sigma K_i C_i} \quad (3)$$

The concentration of intermediates C_i is small due to the low concentration of pollutant and to the limited mineralization rate during the first stages of the reaction. Furthermore, the adsorption constants of the pollutant and of the intermediates, respectively K_a and K_i, may be considered similar. Under these assumptions, Eq. 3 can be reduced to Eq. 4, where $C_{p,0}$ is the initial concentration of pollutant. Notably, the fractional surface coverage of pollutant θ_p is known once K_a is determined.

$$\theta_p = \frac{K_a C_p}{1+K_a C_{p,0}} \quad (4)$$

By substituting this expression of θ_p in Eq. 2 one obtains Eq. 5, where the constant factors are grouped together and defined as k_{obs}.

$$r_H = k\,\theta_p = k\,\frac{K_a}{1+K_a C_{p,0}} C_p = k_{obs}\,C_p \quad (5)$$

Therefore, the reaction rate is determined once the apparent rate constant k_{obs} and the pollutant concentration in the aqueous medium C_p are known. k_{obs} is obtained by interpolating the initial rate from different experimental data while C_p is experimentally measured.

The values of k and K_a may be determined by considering that

$$\frac{1}{k_{obs}} = \frac{1}{k\,K_a} + \frac{C_{P,0}}{k} \quad (6)$$

where all of the parameters, except the initial concentration of pollutant and k_{obs}, are constant. Therefore, plotting the values of $1/k_{obs}$ *vs.* $C_{P,0}$ obtained from runs at different initial 4-NP concentration and applying a linear best fitting procedure, k and K_a are obtained as slope and intercept, respectively.

By solving the differential Eq. 2 under the boundary condition $C_P = C_{P,0}$ at $t = 0$, Eq. 7 is obtained. The latter expresses the exponential decrease of the pollutant concentration during the reaction.

$$C_P = C_{P,0}\,e^{(-k_{obs}\,t)} \quad (7)$$

By adjusting the two parameters K_a and k, the modeled k_{obs} values have been obtained by minimizing the sum of the quadratic errors calculated by difference with the correspondent values obtained from the experimental runs.

3. Results and discussion

3.1.Photocatalytic ozonation of 4-NP solutions

Preliminary tests have been carried out by treating DI water containing 4-NP by means of photocatalysis, ozonation, and photocatalytic ozonation under visible light irradiation.

The benchmark photocatalyst P25 is not able to induce 4-NP degradation (Pikuda et al., 2017) as it was not activated by visible light. The influence of light intensity has been checked by irradiating the reacting mixture only with the internal or with both internal and external LED visible lamps. The activity of the 0.8% N-TiO_2 in the presence of oxygen and ozone irradiated only by the internal LED visible lamps is shown in Figure S2. Results are plotted in terms of concentration of 4-NP and TOC.

When only the internal lamps irradiated the suspension, the 4-NP degradation macroscopically occurred at the same rate by photocatalysis or photocatalytic ozonation (ca. 40% degradation after 10 h). Similar trend may be observed by taking into account the corresponding TOC values. These results do not apparently agree with the reports of the relevant literature (Parrino et al., 2015) where generally the integration of ozonation and photocatalysis presents synergistic effects. In order to understand the reasons of such a result, the same runs with a higher 4-NP concentration (5 ppm) have been performed under both internal and external LED irradiation. Results are shown in Figure 2. In this case the effect of photocatalytic ozonation becomes more evident. In fact, photocatalysis produced 52.5% 4-NP degradation, while 77.8% was achieved by means of photocatalytic ozonation after 7 hours irradiation. Similar trend may be observed by taking into account the corresponding TOC values. The degradation of 4-NP was not observed in dark ozonation.

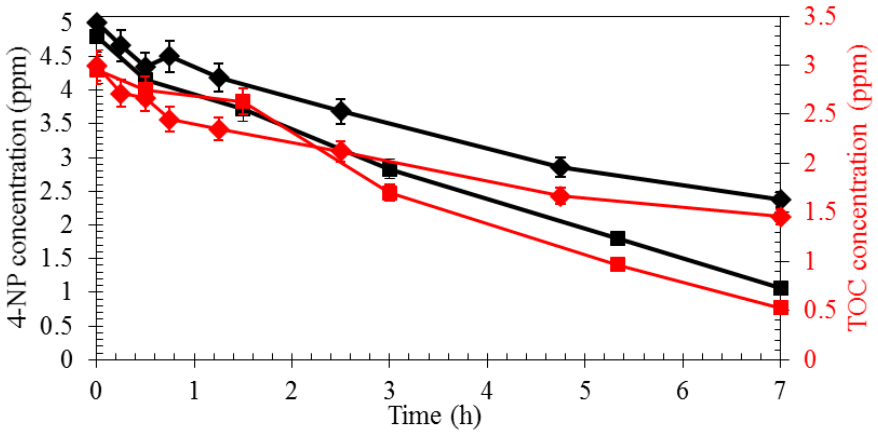

Figure 2. 4-NP (black) and TOC (red) concentrations vs. time during photocatalysis (diamonds), and photocatalytic ozonation (squares) by using both external and internal irradiation systems. Initial 4-NP concentration: 5 ppm.

These results may be explained by considering the radiation field generated through the reacting suspension under the different irradiation conditions. In fact, the internal radiation system produces an intrinsically uneven radiative field due to the attenuation of the light along the radial direction (because of absorption and scattering phenomena) and to the punctual nature of the LED irradiation. On the other hand, the simultaneous external irradiation creates a more uniform radiative field by mitigating the above mentioned light intensity attenuation. The uniformity of the radiative field is a key factor for a correct kinetic analysis of a reacting irradiated suspension (Camera-Roda et al., 2017). Indeed, photons can be considered as reactants, whose concentration is generally not uniform due to the fact that they cannot be "mixed". It is important to stress that recently LED lamps have been widely used as irradiation sources for photocatalytic applications, due to their low cost, energy consumption, and good versatility. In the case of reactors irradiated only annularly, the local values of the relevant kinetic parameters, whose knowledge derives by the demanding solution of the radiative

transport equation, significantly differ from the corresponding average values which, on the other hand, are the only experimentally accessible. Therefore, using the experimental values in this situation would generate an incorrect kinetic analysis. Camera-Roda et al. (2016) pointed out that the experimental values of the reaction rate closely approach the local ones, by increasing the uniformity of the radiant field and working at a low value of the suspension optical thickness. Accordingly, by using both internal and external visible light sources, the radiative field becomes more uniform and the reactor volume is more efficiently irradiated. In these conditions the TiO_2 induced ozone activation becomes evident as shown in Figure 2. The more electrophilic character of ozone with respect to oxygen makes it a better electron acceptor compared to oxygen, giving rise to ozonide radical anions according to Eq. 8. Incidentally, the advantage of having ozone rather than oxygen reacting with conduction band electrons might be not evident in those cases where Eq. 8 is not the reaction limiting step: such event occurs in the presence of a limited extent of conduction band electrons, which is likely if the photon flux is insufficient. Upon production of the ozonide radical, by protonation (Eq. 9), oxygen and one hydroxyl radical per absorbed photon (Eq. 10) can be generated.

$$O_3 + e^- \rightarrow O_3^{\bullet -} \quad (8)$$

$$O_3^{\bullet -} + H^+ \rightarrow HO_3^{\bullet} \quad (9)$$

$$HO_3^{\bullet} \rightarrow O_2 + {}^{\bullet}OH \quad (10)$$

On the other hand three photons are required to produce one hydroxyl radical through oxygen reduction, as shown in Eqs. 11-14.

$$3O_2 + 3e^- \rightarrow 3O_2^{\bullet -} \quad (11)$$

$$2O_2^{\bullet-} + 2H^+ \rightarrow 2HO_2^{\bullet} \quad (12)$$

$$2HO_2^{\bullet} \rightarrow H_2O_2 + O_2 \quad (13)$$

$$H_2O_2 + O_2^{\bullet-} \rightarrow {}^{\bullet}OH + OH^- + O_2 \quad (14)$$

These considerations, often reported in the relevant literature (Agustina et al., 2005), justify the improved degradation efficiency of photocatalytic ozonation with respect to the separate technologies.

Once optimized the irradiation conditions, the assessment of 4-NP oxidation was carried out by L-H kinetics applied to photocatalysis and photocatalytic ozonation, as detailed in the experimental section. Even if it is the most used model to assess kinetics of photocatalytic reactions, this model presents also a number of drawbacks, which have been highlighted in the past years by a number of scholars (Pelizzetti et al., 1993). One of the most common critical point is the saturation of the active sites which – according to L-H model – should bring to a plateau in the reaction rate by increasing the initial concentration of the reactant, whereas experimental evidence shows often a continuous rate increase (Vione et al., 2005).

Furthermore, it is well known that photocatalytic experimental values may be satisfactorily fit by various kinetic models. Therefore, it is worth to note that the kinetic parameters hereby provided do not possess certain physical significance and should be rather considered adjustable parameters useful for prediction purposes.

Figures 3 and S3 show that the above discussed model satisfactorily describes experimental runs at different 4-NP initial concentration (8, 5, 3, and 1 ppm) for photocatalytic ozonation and photocatalysis, respectively. After 7 hours photocatalysis afforded 4-NP degradation ranging

between 49 and 76%, while photocatalytic ozonation between 69 and 87%, depending on the initial 4-NP concentration.

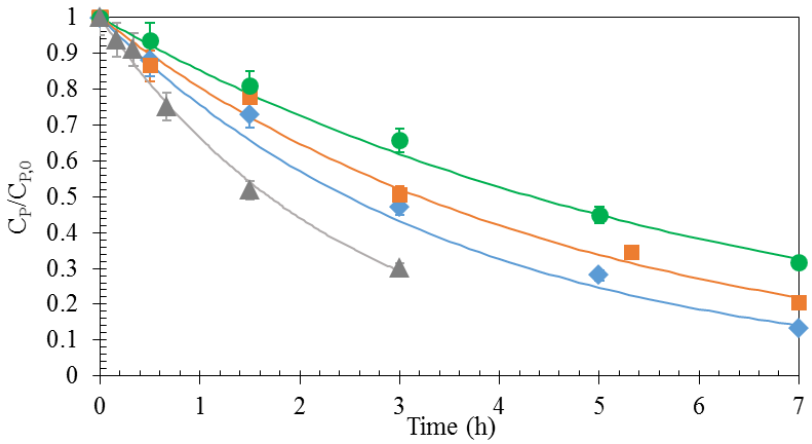

Figure 3. Normalized 4-NP concentration vs time curves from the L-H model and experimental points from the photocatalytic ozonation runs under internal and external visible light irradiation. Initial 4-NP concentrations: 8ppm (green circles), 5 ppm (orange squares), 3 ppm (blue diamonds) and 1 ppm (grey triangles). Lines represent the L-H model.

The model yielded values of $k = 8.63 \times 10^{-8}$ mol m^{-2} h^{-1} and $K_a = 1.12 \times 10^{5}$ M^{-1} for the photocatalytic treatment, and $k = 1.73 \times 10^{-7}$ mol m^{-2} h^{-1} and $K_a = 4.06 \times 10^{4}$ M^{-1} for photocatalytic ozonation. Notably, the rate constant is almost doubled, while the 4-NP adsorption constant is one order of magnitude smaller when photocatalysis is performed in the presence of ozone with respect to oxygen.

Given the previous study on the samples of TiO_2 here employed (Pikuda et al., 2017), its reusability has not been assessed in the present study.

3.2. Photocatalytic ozonation of the grey water of Masdar City

Photocatalytic ozonation under visible light in the presence of 0.8% N-TiO_2 has been performed on Masdar City grey water diluted in a ratio 1:20. Due to the complexity of the matrix the degradation of pollutants was monitored only in terms of TOC.

Preliminary tests demonstrated that the simultaneous presence of visible light and of the 0.8% N-TiO_2 photocatalyst was necessary for the reaction to occur (Figures S4 and 4).

Indeed, irradiating the grey water but in the absence of the 0.8% N-TiO_2 and with oxygen or ozone bubbling, did not produce appreciable TOC decrease during 12 hours of treatment. Analogous results have been obtained in dark conditions. Under visible light irradiation the benchmark photocatalyst P25 did not show any activity even in the presence of ozone, but slowly released the organic impurities adsorbed on its surface, so that the TOC increased during time as shown in Figure S4. Notably, when the catalyst was present in the reacting suspension, organics adsorbed almost instantaneously on its surface so that when the lamp was switched on the initial concentration in liquid phase was lower than for the runs in homogeneous phase.

On the other hand, the TOC concentration of the grey water decreased by applying photocatalysis or photocatalytic ozonation under visible light irradiation and in the presence of 0.8% N-TiO_2. Results are shown in Figure 4.

Several runs have been performed starting from different initial TOC concentrations obtained by varying the dilution ratio between 1:7.5 and 1:40. The TOC values against reaction time are displayed in Figures 5 and S5, for photocatalytic ozonation and photocatalysis, respectively, in the presence of 0.8% N-TiO_2 and under visible light irradiation. It is possible to observe the initial increase of TOC concentration soon after switching on the light, because of photodesorption of species previously adsorbed in the dark stage, in agreement with previous literature (Boyjoo et al., 2012; El Saliby et al., 2012; Hidaka et al., 2010). This behavior could

not be satisfactorily predicted by means of a proper kinetic model due to the complexity of the matrix and to the specific surface features generated upon light induced excitation of the photocatalyst.

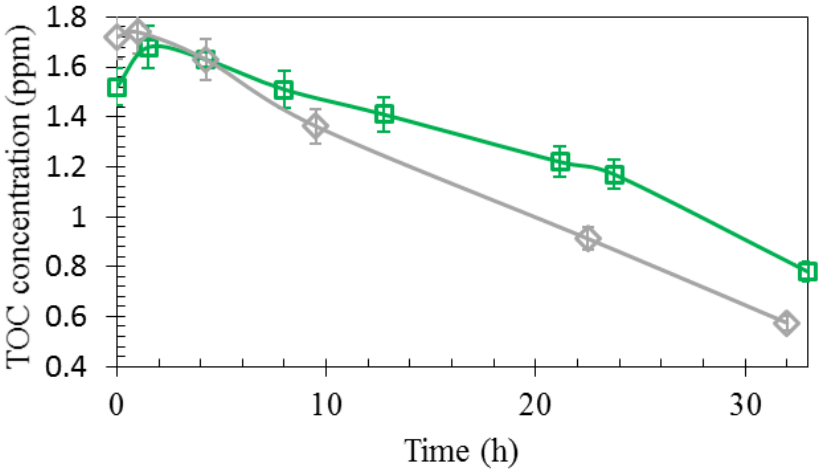

Figure 4. TOC concentration vs time for the degradation of a grey water solution (diluted 1:20) through photocatalysis (green squares) and photocatalytic ozonation (grey diamonds) under internal and external visible light irradiation.

The TOC decrease reached 25.7% in the case of photocatalysis applied to a 1:7.5 diluted grey water and 54.9% for the photocatalytic ozonation treatment on a 1:40 diluted matrix. Figures 5 and S5 also show the different trends obtained at different initial concentrations.

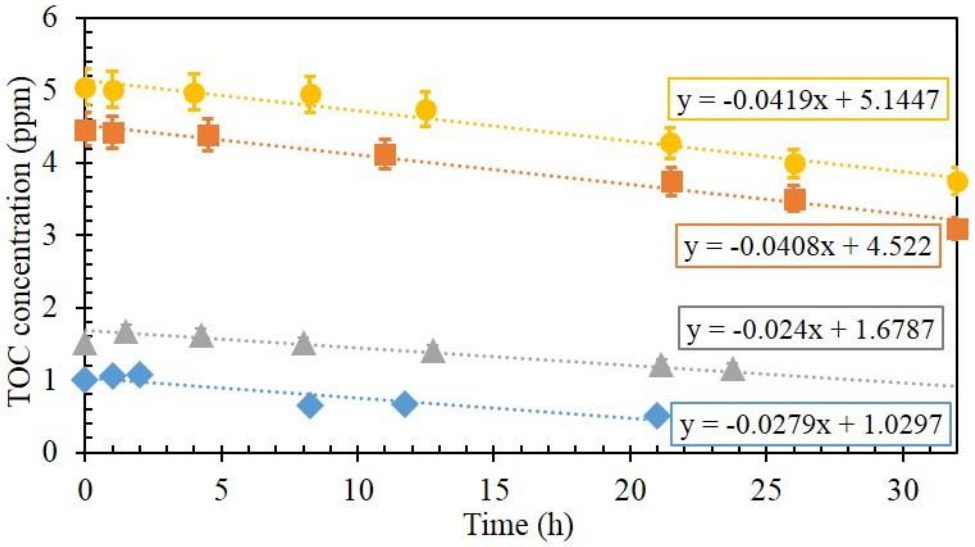

Figure 5. TOC concentration vs time for the photocatalytic ozonation treatment of grey water under internal and external visible light irradiation. Dilution ratios: 1:7.5 (circles), 1:10 (squares), 1:20 (triangles) and 1:40 (diamonds).

The complexity of the grey water matrix and the photodesoption phenomena occurring soon after the start of irradiation did not allow to apply the Langmuir-Hinshelwood model successfully by using the TOC trends.

The effect of photocatalytic ozonation was tested by a total bacteria count (TBC) analysis, performed before and after the treatments of photocatalytic ozonation. The bacterial amount in the 1:20 diluted grey water sample was found to be 3.75×10^4 CFU/mL. After 32 h of photocatalytic ozonation treatment, the TBC count was found to decrease from an initial concentration 3.75×10^4 CFU/mL to 10 CFU/mL. The reactive oxygen species leads to loss of cell membrane potential causing the oxidative damage to cellular components and finally causing the lysis of the microorganisms (Mecha et al., 2017). This result is significant as it implies that photocatalytic ozonation not only allows the abatement of the organic load in grey water but also

411 promotes the disinfection of the effluent thus offering the possibility of water reuse. It is worth
412 noting that, in the absence of ozone, no decrease in the TBC was achieved.

413 In order to get information on the modifications involving the inorganic species present in the
414 grey water, ion chromatography was performed at fixed intervals of time during the
415 photocatalysis and photocatalytic ozonation runs. This analysis is relevant as some inorganic
416 species present in the grey water or formed upon ozonation treatment possess high toxicity. This
417 is the case of ammonia or bromate ions. In particular bromate ions are generated by ozone-
418 induced oxidation of bromide ions and they represent a great concern due to their toxic,
419 mutagenic, and carcinogenic effects. Indeed, the suggested exposure safety value of bromate is 3
420 mg L^{-1} (Hutchinson et al., 1997) and the concentrations in drinking water associated with
421 upper-bound excess lifetime cancer risks of 10^{-4}, 10^{-5}, and 10^{-6} are 20, 2 and 0.2 μg/L,
422 respectively (U.S. EPA., 2001)

423 Figure S6 shows the concentration of selected ions during photocatalytic ozonation runs.
424 Results obtained for the photocatalytic treatment are reported in the supplementary information
425 (Figure S7), as they are similar to those hereby reported for the photocatalytic ozonation, as far
426 as the formation of sulphate, nitrate and ammonia are concerned. The only exception is the
427 behavior of bromide ions, whose concentration, unlike in photocatalytic ozonation, does not vary
428 macroscopically during the photocatalytic treatment.

429 Photocatalytic ozonation promotes the oxidation of the inorganic ions present in water to
430 higher oxidation states (Parrino et al., 2015). This is the case of sulphur or bromine containing
431 compounds which are oxidized to sulphate and bromate, respectively. As above mentioned,
432 while sulphate ions do not pose relevant environmental or health problems, this is not the case of
433 bromate ions. Parrino et al. (2015) proposed a strategy assessment by alternating photocatalytic

ozonation and photocatalysis in order to control the production of bromate. Similar approach may be used also in this case, although this problem is beyond the scope of the present work.

Ca^{2+} is already in its highest oxidation state but its concentration decreased during photocatalytic ozonation. This is probably due to the binding of Ca^{2+} on the TiO_2 surface reported in literature (Tang et al., 2010), since the precipitation of alkali compounds can be ruled out in the present case given that the pH of grey water is ca. 5.0 (Table S1).

The behavior of nitrogen species is more complex and depends on different factors, pH, temperature and the interaction of nitrogen species with other metabolites, as reported by the relevant literature (Zhu et al., 2005). Figure S6 shows that whereas the initial concentration of ammonium ion was very small, 0.006 ppm, it sharply increased during the photocatalytic ozonation runs. The low concentration of ammonium ions can be due to the presence of the bacteria in the grey water, especially nitrifying bacteria, since ammonium ion is the preferred nitrogen source for most of the bacteria, despite of its cytotoxicity, and is diffused across the bacterial cell membrane by the ammonium transport (Amt) family of proteins (Müller et al., 2006). However, during the photocatalytic ozonation runs, we observed an increase in the concentration of ammonium, which may be related to the lysis of bacteria above mentioned, rather than to reactions directly related to photocatalytic ozonation. Accordingly, the metabolic products generated and stored by the bacteria present in the grey water might be released in the aqueous medium once the microorganisms were destroyed by photocatalytic ozonation. This hypothesis is also supported by the above reported TBC results. Moreover, while the concentration of nitrate ions increased, the concentration of nitrite ions decreased during the photocatalytic ozonation runs, highlighting how the photocatalytic oxidation of ammonium ions produces nitrite and nitrate *via* series reactions, as reported in literature (Zhu et al., 2005).

3.3 eMBR-photocatalytic ozonation integrated system

Selected photocatalytic ozonation runs were carried out on a grey water previously treated by means of eMBR accordingly to a previous report (Hasan et al., 2014). The effluent downstream to the eMBR treatment has been characterized and the main characteristics are summarized in Table S2.

Samples of raw municipal grey water were collected from Masdar City and were firstly treated by the eMBR (as a secondary treatment) before photocatalytic ozonation (as a tertiary treatment). The concentration of pollutants in the grey water feed was 420±130 ppm, 4.2±3.0 ppm, 14.6±7.4 ppm, 1.95±0.5 ppm, 2.7±0.3 ppm of COD, PO_4^{3-}, NH_4^+, Zn, and Fe, respectively. The removal of COD, PO_4^{3-}, NH_4^+, Fe, and Zn were reported to be 94.8±1.4%, 97.1±2.1%, 83.7±5.8%, 95.2±0.7, and 98.8±0.3%, respectively, after eMBR treatment operated at a current density of 10 A m^{-2}. eMBR effluent composition was 23.0±4.2, 1.3±0.7, 2.5±0.7, 0.11±0.03, and 0.03±0.02 of COD, PO_4^{3-}, NH_4^+, Zn, and Fe, respectively (Ahmed and Hasan, 2017).

The eMBR treatment produced a drastic decrease of the TOC concentration so that further dilution prior to photocatalytic ozonation treatment was not required. Photocatalysis and photocatalytic ozonation have been performed on this effluent in the presence of 0.8% N-TiO_2 under visible light irradiation. The TOC concentration profile during irradiation is shown in Figure 7.

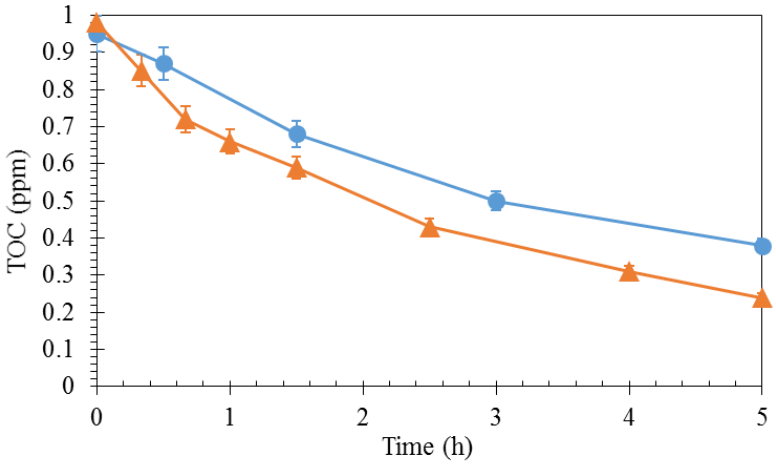

Figure 7. TOC variation vs time for the photocatalytic (blue circles) and photocatalytic ozonation (orange triangles) of an eMBR effluent under internal and external visible light irradiation.

Around 60% and 74% of mineralization have been achieved after 5 hours of treatment with photocatalysis and photocatalytic ozonation, respectively. By comparing these results with those obtained without the preliminary membrane treatment, it can be concluded that photocatalysis and photocatalytic ozonation are more efficient if applied downstream to an eMBR treatment. This is mainly due to the fact that eMBR process limits the turbidity of the stream and significantly abates the organic load of the stream. On the other hand, photocatalysis and photocatalytic ozonation allow to reach a deeper level of depuration and disinfection with respect to the sole eMBR with a minimum energy surplus. In fact, these process may be activated by cheap and abundant solar light which is mainly constituted by visible light (Garlisi et al., 2015). Furthermore, the combination of the two technologies allowed to treat without any dilution the grey water with significant advantages in terms of costs and water consume.

These preliminary results on coupling eMBR and photocatalysis or photocatalytic ozonation are promising and further investigations are ongoing in order to improve their integration degree and enhance the overall process efficiency.

3.4. Open issues and future developments

Even if this study demonstrated the possibility to perform photocatalytic ozonation under UV-free visible radiation to treat grey water, in particular downstream to an eMBR unit, some issues remain open and further advances are needed to elevate the proof of concept to applications. First of all an optimization of the whole system would be required to make the process attractive from a practical point of view; in particular it is possible to work on catalyst loading, light radiation intensity, ozone concentration and the reactor itself to reduce reaction time. In particular, the optimization of the amount of required ozone and of the intensification between the two considered technologies could give rise to significant operative costs reduction.

A relevant point to be addressed is the ability of photocatalytic ozonation to abate trace amounts of contaminants of environmental concern, which are recalcitrant to biological treatment and require a detailed chemical characterization of the matrix and suitable monitoring techniques.

Even if TOC values directly relate the efficiency of the treatment with the presence of organic carbon, thus being more appropriate in the present scientific report, the current legislation requires to compare indirect parameters such as BOD (biochemical oxygen demand) and/or COD (chemical oxygen demand) with the imposed limits for effluent disposal or reuse. This issue must be considered in future reports mainly addressed to the technical assessment of the proposed technology. The economic implications of a tertiary treatment downstream to a

biological one do not have to be forgotten and decision on whether implementing it must be taken based on the characteristics of the treated effluent and its final fate, by addressing the cost of ozone in the overall balance.

4. Conclusions

Photocatalysis and photocatalytic ozonation have been applied to the purification and disinfection of the grey water of Masdar City. Preliminary results on 4-NP solutions highlighted the essential role of a uniform radiative field distribution and allowed to set the operative conditions for the treatment of grey water. Photocatalytic ozonation under visible light allowed to decrease the TOC content of grey water up to 60% and to reduce of ca. 97% the total bacterial load. The extent of purification reached ca. 80% if the photocatalytic ozonation occurred downstream to a preliminary electro-membrane bioreactor (eMBR). Coupling the two processes enhanced the global efficiency. In fact, the eMBR treatment decreases the turbidity and the organic load of the effluent entering the photocatalytic ozonation treatment which in turn enhances the extent of purification and disinfection. The presented results are promising and probably worth of further investigations with regard to their practical implications, as detailed in the previous section.

Acknowledgments

Authors would like to thank Masdar Institute of Science and Technology (now part of Khalifa University of Science and Technology) for financial support (Grant No. SSG2015-000024). Our appreciation also goes to Dr. L. Yousef and Dr. A. Yousef (Khalifa University of Science and Technology) for enabling the use of their lab facilities to carry out the TBC analysis.

538

539 **References**

540 Agustina, T.E., Ang, H.M., Vareek, V.K., 2005. A review of synergistic effect of photocatalysis
541 and ozonation on wastewater treatment. J. Photochem. Photobiol. C Photochem. Rev. 6,
542 264–273. https://doi.org/10.1016/j.jphotochemrev.2005.12.003

543 Ahmadi, M., Ghanbari, F., Moradi, M., 2015. Photocatalysis assisted by peroxymonosulfate and
544 persulfate for benzotriazole degradation: effect of pH on sulfate and hydroxyl radicals.
545 Water Sci. Technol. 72, 2095–2102. https://doi.org/10.2166/wst.2015.437

546 Ahmed, M.A., Hasan, S.W., 2017. Fe and Zn removal from industrial wastewater using
547 electrically-enhanced membrane bioreactor. Desalin. Water Treat. 93, 9–21.
548 https://doi.org/10.5004/dwt.2017.21305

549 Ardizzone, S., Cappelletti, G., Meroni, D., Spadavecchia, F., 2011. Tailored TiO_2 layers for the
550 photocatalytic ozonation of cumylphenol, a refractory pollutant exerting hormonal activity.
551 Chem. Commun. 47, 2640–2642. https://doi.org/10.1039/c0cc05134a

552 Augugliaro, V., Loddo, V., Pagliaro, M., Palmisano, G., Palmisano, L., 2010. Clean by Light
553 Irradiation. Royal Society of Chemistry, Cambridge.
554 https://doi.org/10.1039/9781849732031

555 Bernabeu, A., Vercher, R.F., Santos-Juanes, L., Simón, P.J., Lardín, C., Martínez, M.A., Vicente,
556 J.A., González, R., Llosá, C., Arques, A., Amat, A.M., 2011. Solar photocatalysis as a
557 tertiary treatment to remove emerging pollutants from wastewater treatment plant effluents.
558 Catal. Today 161, 235–240. https://doi.org/10.1016/J.CATTOD.2010.09.025

559 Borges, M.E., Hernández, T., Esparza, P., 2014. Photocatalysis as a potential tertiary treatment
560 of urban wastewater: new photocatalytic materials. Clean Technol. Environ. Policy 16,

431–436. https://doi.org/10.1007/s10098-013-0637-z

Boyjoo, Y., Ang, M., Pareek, V., 2012. Photocatalytic Treatment of Shower Water Using a Pilot Scale Reactor. Int. J. Photoenergy 2012, 1–7. https://doi.org/10.1155/2012/578916

Camera-Roda, G., Augugliaro, V., Cardillo, A.G., Loddo, V., Palmisano, L., Parrino, F., Santarelli, F., 2016. A reaction engineering approach to kinetic analysis of photocatalytic reactions in slurry systems. Catal. Today 259, 87–96. https://doi.org/10.1016/j.cattod.2015.05.007

Camera-Roda, G., Loddo, V., Palmisano, L., Parrino, F., 2018. Photocatalytic ozonation for sustainable aquaculture: a long-term test in a seawater aquarium. J. Hazard. Mater.

Camera-Roda, G., Loddo, V., Palmisano, L., Parrino, F., 2017. Guidelines for the assessment of the rate law of slurry photocatalytic reactions. Catal. Today 281, 221–230. https://doi.org/10.1016/j.cattod.2016.06.050

Cataldo, S., Ianni, A., Loddo, V., Mirenda, E., Palmisano, L., Parrino, F., Piazzese, D., 2016. Combination of advanced oxidation processes and active carbons adsorption for the treatment of simulated saline wastewater. Sep. Purif. Technol. 171, 101–111. https://doi.org/10.1016/j.seppur.2016.07.026

Dolat, D., Mozia, S., Ohtani, B., Morawski, A.W., 2013. Nitrogen, iron-single modified (N-TiO_2, Fe-TiO_2) and co-modified (Fe,N-TiO_2) rutile titanium dioxide as visible-light active photocatalysts. Chem. Eng. J. 225, 358–364. https://doi.org/10.1016/J.CEJ.2013.03.047

El Saliby, I., Shahid, M., McDonagh, A., Shon, H.K., Kim, J.-H., 2012. Photodesorption of organic matter from titanium dioxide particles in aqueous media. J. Ind. Eng. Chem. 18, 1774–1780. https://doi.org/10.1016/J.JIEC.2012.04.002

Ensano, B.M.B., Borea, L., Naddeo, V., Belgiorno, V., de Luna, M.D.G., Ballesteros, F.C., 2016.

584 Combination of Electrochemical Processes with Membrane Bioreactors for Wastewater
585 Treatment and Fouling Control: A Review. Front. Environ. Sci. 4, 57.
586 https://doi.org/10.3389/fenvs.2016.00057
587 Garcia-Segura, S., Brillas, E., 2017. Applied photoelectrocatalysis on the degradation of organic
588 pollutants in wastewaters. J. Photochem. Photobiol. C Photochem. Rev. 31, 1–35.
589 https://doi.org/10.1016/j.jphotochemrev.2017.01.005
590 Garlisi, C., Scandura, G., Alabi, A., Aderemi, O., Palmisano, G., 2015. Self-Cleaning Coatings
591 Activated by Solar and Visible Radiation. J. Adv. Chem. Eng. 5.
592 https://doi.org/10.4172/2090-4568.1000e103
593 Gimeno, O., Rivas, F.J., Beltrán, F.J., Carbajo, M., 2007. Photocatalytic Ozonation of Winery
594 Wastewaters. J. Agric. Food Chem. 55, 9944–9950. https://doi.org/10.1021/jf072167i
595 Giwa, A., Ahmed, I., Hasan, S.W., 2015. Enhanced sludge properties and distribution study of
596 sludge components in electrically-enhanced membrane bioreactor. J. Environ. Manage. 159,
597 78–85. https://doi.org/10.1016/j.jenvman.2015.05.035
598 Giwa, A., Hasan, S.W., 2015a. Numerical modeling of an electrically enhanced membrane
599 bioreactor (MBER) treating medium-strength wastewater. J. Environ. Manage. 164, 1–9.
600 https://doi.org/10.1016/j.jenvman.2015.08.031
601 Giwa, A., Hasan, S.W., 2015b. Theoretical investigation of the influence of operating conditions
602 on the treatment performance of an electrically-induced membrane bioreactor. J. Water
603 Process Eng. 6, 72–82. https://doi.org/10.1016/j.jwpe.2015.03.004
604 Hasan, S.W., Electorowicz, M., Oleszkiewicz, J.A., 2014. Start-up period investigation of pilot-
605 scale submerged membrane electro-bioreactor (SMEBR) treating raw municipal
606 wastewater. Chemosphere 97, 71–77. https://doi.org/10.1016/j.chemosphere.2013.11.009

607 Hasan, S.W., Elektorowicz, M., Oleszkiewicz, J.A., 2012. Correlations between trans-membrane
608 pressure (TMP) and sludge properties in submerged membrane electro-bioreactor (SMEBR)
609 and conventional membrane bioreactor (MBR). Bioresour. Technol. 120, 199–205.
610 https://doi.org/10.1016/j.biortech.2012.06.043
611 Hidaka, H., Oyama, T., Horiuchi, T., Koike, T., Serpone, N., 2010. Photo-induced oxidative
612 synergistic degradation of mixed anionic/cationic surfactant systems in aqueous dispersions.
613 A detailed study of the DBS/HTAB system. Appl. Catal. B Environ. 99, 485–489.
614 https://doi.org/10.1016/J.APCATB.2010.06.041
615 Hutchinson, T.H., Hutchings, M.J., Moore, K.W., 1997. A Review of the effects of bromate on
616 aquatic organisms and toxicity of bromate to oyster (Crassostrea gigas) embryos.
617 Ecotoxicol. Environ. Saf. 38, 238–243. https://doi.org/10.1006/eesa.1997.1584
618 Kisch, H., 2014. Semiconductor photocatalysis: Principles and applications. Wiley-VCH Verlag
619 GmbH & Co. KGaA, Weinheim, Germany. https://doi.org/10.1002/9783527673315.ch1
620 León, D.E., Zúñiga-Benítez, H., Peñuela, G.A., Mansilla, H.D., 2017. Photocatalytic Removal of
621 the Antibiotic Cefotaxime on TiO2 and ZnO Suspensions Under Simulated Sunlight
622 Radiation. Water, Air, Soil Pollut. 228, 361. https://doi.org/10.1007/s11270-017-3557-4
623 Maddila, S., Oseghe, E.O., Jonnalagadda, S.B., 2016. Photocatalyzed ozonation by Ce doped
624 TiO_2 catalyst degradation of pesticide Dicamba in water. J. Chem. Technol. Biotechnol. 91,
625 385–393. https://doi.org/10.1002/jctb.4583
626 Mano, T., Nishimoto, S., Kameshima, Y., Miyake, M., 2015. Water treatment efficacy of various
627 metal oxide semiconductors for photocatalytic ozonation under UV and visible light
628 irradiation. Chem. Eng. J. 264, 221–229. https://doi.org/10.1016/j.cej.2014.11.088
629 Mecha, A.C., Onyango, M.S., Ochieng, A., Momba, M.N.B., 2017. Evaluation of synergy and

630 bacterial regrowth in photocatalytic ozonation disinfection of municipal wastewater. Sci.
631 Total Environ. 601–602, 626–635. https://doi.org/10.1016/J.SCITOTENV.2017.05.204
632 Mena, E., Rey, A., Acedo, B., Beltrán, F.J., Malato, S., 2012. On ozone-photocatalysis
633 synergism in black-light induced reactions: Oxidizing species production in photocatalytic
634 ozonation versus heterogeneous photocatalysis. Chem. Eng. J. 204–206, 131–140.
635 https://doi.org/10.1016/j.cej.2012.07.076
636 Müller, T., Walter, B., Wirtz, A., Burkovski, A., 2006. Ammonium Toxicity in Bacteria. Curr.
637 Microbiol. 52, 400–406. https://doi.org/10.1007/s00284-005-0370-x
638 Ohno, T., Tsubota, T., 2010. Development and Sensitization of N- or S-Doped TiO_2
639 Photocatalysts, in: Environmentally Benign Photocatalysts. Springer, New York, NY, pp.
640 253–275. https://doi.org/10.1007/978-0-387-48444-0_11
641 Pan, Z., Cai, Q., Luo, Q., Li, X., 2015. Photocatalytic Ozonation of Oxalic Acid Over Cu(II)-
642 Grafted TiO_2 Under Visible Light Irradiation. Synth. React. Inorganic, Met. Nano-Metal
643 Chem. 45, 447–450. https://doi.org/10.1080/15533174.2013.841207
644 Parrino, F., Camera-Roda, G., Loddo, V., Augugliaro, V., Palmisano, L., 2015. Photocatalytic
645 ozonation: Maximization of the reaction rate and control of undesired by-products. Appl.
646 Catal. B Environ. 178, 37–43. https://doi.org/10.1016/j.apcatb.2014.10.081
647 Parrino, F., Camera-Roda, G., Loddo, V., Palmisano, G., Augugliaro, V., 2014. Combination of
648 ozonation and photocatalysis for purification of aqueous effluents containing formic acid as
649 probe pollutant and bromide ion. Water Res. 50, 189–199.
650 https://doi.org/10.1016/j.watres.2013.12.001
651 Pelaez, M., Nolan, N.T., Pillai, S.C., Seery, M.K., Falaras, P., Kontos, A.G., Dunlop, P.S.M.,
652 Hamilton, J.W.J., Byrne, J.A., O'Shea, K., Entezari, M.H., Dionysiou, D.D., 2012. A

review on the visible light active titanium dioxide photocatalysts for environmental applications. Appl. Catal. B Environ. 125, 331–349. https://doi.org/10.1016/j.apcatb.2012.05.036

Pelizzetti, E., Minero, C., Borgarello, E., Tinucci, L., Serpone, N., 1993. Photocatalytic activity and selectivity of titania colloids and particles prepared by the sol-gel technique: photooxidation of phenol and atrazine. Langmuir 9, 2995–3001. https://doi.org/10.1021/la00035a043

Pikuda, O., Garlisi, C., Scandura, G., Palmisano, G., 2017. Micro-mesoporous N-doped brookite-rutile TiO_2 as efficient catalysts for water remediation under UV-free visible LED radiation. J. Catal. 346, 109–116. https://doi.org/10.1016/j.jcat.2016.12.010

Tang, F., Xu, B., Shi, H., Qiu, J., Fan, Y., 2010. The poisoning effect of Na^+ and Ca^{2+} ions doped on the V_2O_5/TiO_2 catalysts for selective catalytic reduction of NO by NH_3. Appl. Catal. B Environ. 94, 71–76. https://doi.org/10.1016/j.apcatb.2009.10.022

Tseng, D.-H., Juang, L.-C., Huang, H.-H., 2012. Effect of Oxygen and Hydrogen Peroxide on the Photocatalytic Degradation of Monochlorobenzene in TiO_2 Aqueous Suspension. Int. J. Photoenergy 2012, 1–9. https://doi.org/10.1155/2012/328526

U.S. EPA., 2001. Toxicology review of bromate (CAS No. 15541-45-4) in support of Integrated Risk Information System (IRIS). Washington, DC.

Vilar, V.J.P., Amorim, C.C., Li Puma, G., Malato, S., Dionysiou, D.D., 2017. Intensification of photocatalytic processes for niche applications in the area of water, wastewater and air treatment. Chem. Eng. J. 310, 329–330. https://doi.org/10.1016/j.cej.2016.11.131

Vione, D., Minero, C., Maurino, V., Carlotti, M.E., Picatonotto, T., Pelizzetti, E., 2005. Degradation of phenol and benzoic acid in the presence of a TiO2-based heterogeneous

photocatalyst. Appl. Catal. B Environ. 58, 79–88. https://doi.org/10.1016/J.APCATB.2004.11.018

Wang, S., Shiraishi, F., Nakano, K., 2002. A synergistic effect of photocatalysis and ozonation on decomposition of formic acid in an aqueous solution. Chem. Eng. J. 87, 261–271. https://doi.org/10.1016/S1385-8947(02)00016-5

Zhu, X., Castleberry, S.R., Nanny, M.A., Butler, E.C., 2005. Effects of pH and catalyst concentration on photocatalytic oxidation of aqueous ammonia and nitrite in titanium dioxide suspensions. Environ. Sci. Technol. 39, 3784–91.

Zou, L., Zhu, B., 2008. The synergistic effect of ozonation and photocatalysis on color removal from reused water. J. Photochem. Photobiol. A Chem. 196, 24–32. https://doi.org/10.1016/j.jphotochem.2007.11.008